Nanoscale

PAPER

View Article Online
View Journal | View Issue

Cite this: *Nanoscale*, 2014, **6**, 11835

Atomically resolved orientational ordering of C_{60} molecules on epitaxial graphene on Cu(111)†

Minbok Jung,[ab] Dongbin Shin,[c] So-Dam Sohn,[ab] Soon-Yong Kwon,[a] Noejung Park[c] and Hyung-Joon Shin*[ab]

A detailed understanding of interactions between molecules and graphene is one of the key issues for tailoring the properties of graphene-based molecular devices, because the electronic and structural properties of molecular layers on surfaces are determined by intermolecular and molecule–substrate interactions. Here, we present the atomically resolved experimental measurements of the self-assembled fullerene molecules on single-layer graphene on Cu(111). Fullerene molecules form a (4 × 4) superstructure on graphene/Cu(111), revealing only single molecular orientation. We can resolve the exact adsorption site and the configuration of fullerene by means of low-temperature scanning tunnelling microscopy (LT-STM) and density functional theory (DFT) calculations. The adsorption orientation can be explained in terms of the competition between intermolecular interactions and molecule–substrate interactions, where strong Coulomb interactions among the fullerenes determine the in-plane orientation of the fullerene. Our results provide important implications for developing carbon-based organic devices using a graphene template in the future.

Received 13th June 2014
Accepted 12th August 2014

DOI: 10.1039/c4nr03249g

www.rsc.org/nanoscale

1. Introduction

Since the discovery of graphene, carbon-based materials including other types of carbon allotropes such as fullerene (C_{60}) and one-dimensional carbon nanotubes (CNTs) have attracted much attention due to their distinctive electronic and physical properties as well as their potential for use as building blocks for molecular electronic devices.[1–4] The scale of electronic components continues to shrink to the point that it is now on the scale of a few tens of nanometres. We expect that electronic devices on such a scale can be realized with molecular components and this encourages research leading to a greater understanding of the fundamentals of molecular systems. In particular, fullerene and its derivatives have been considered as promising organic materials in many applications such as field effect transistors,[5] organic solar cells,[6] and organic light emitting diodes.[7] Due to its potential for use in various applications, a considerable amount of effort has been made in an effort to understand the fundamental physical and chemical properties of the fullerene molecule. Given that most applications of C_{60} have been assessed in the form of a molecular layer on a supporting substrate, much of this effort has thus far been focused on gaining precise information about the behaviour of fullerene on various surfaces. In order to realize carbon-based organic electronic devices using a graphene template, it is of significance to understand the equilibrium configurations of molecules on graphene and the interaction between certain molecules and graphene.

The synthesis of graphene on Cu by the chemical vapour deposition (CVD) method is one of the most popular methods used to obtain large-sized graphene.[8] However, there has been no investigation of C_{60} molecules on graphene/Cu regarding the precise adsorption sites, adsorption structure, and the detailed relationships between graphene–substrate and fullerene–graphene. In this paper, we report a low-temperature scanning tunnelling microscopy (STM) study of self-assembled fullerene molecules on graphene/Cu(111) combined with first-principles density functional theory (DFT) calculations. By preparing sub-monolayer C_{60} molecules on graphene/Cu(111), we can successfully resolve the exact adsorption site and orientation of individual fullerenes by means of STM. Interestingly, all of the fullerenes are shown to be arranged in a single orientation. We find that the C_{60}–C_{60} Coulomb interaction and the C_{60}–graphene interaction play important roles in determining the configuration of self-assembled fullerenes.

[a]*School of Materials Science and Engineering, Center for Multidimensional Carbon Materials and Low Dimensional Carbon Materials Center, Ulsan National Institute of Science and Technology (UNIST), UNIST-gil 50, Ulsan 689-798, Republic of Korea. E-mail: shinhj@unist.ac.kr; Fax: +82-52-217-2309; Tel: +82-52-217-2329*

[b]*KIST-UNIST Ulsan Center for Convergent Materials, Ulsan National Institute of Science and Technology (UNIST), UNIST-gil 50, Ulsan 689-798, Republic of Korea*

[c]*Department of Physics, Center for Multidimensional Carbon Materials and Low Dimensional Carbon Materials Center, Ulsan National Institute of Science and Technology (UNIST), UNIST-gil 50, Ulsan 689-798, Republic of Korea*

† Electronic supplementary information (ESI) available. See DOI: 10.1039/c4nr03249g

2. Methods

2.1 Experimental details

The experiments were performed using an ultrahigh-vacuum low-temperature scanning tunnelling microscope (SPECS, JT-STM). The base pressure of our system was less than 4.7×10^{-11} Torr. The Cu(111) single crystal was cleaned by several cycles of Ar^+ sputtering and annealing. After the sample cleaning process, single-layer graphene was synthesized by an Ar-assisted growth method.[9] Ethylene gas (99.8%, Sigma-Aldrich) was leaked into the preparation chamber at a pressure of 1.5×10^{-4} Torr followed by the introduction of Ar gas to a total pressure of 1.5 mTorr. The temperature of the substrate was kept at 1073 K. After confirming single-layer graphene by STM, we deposited C_{60} molecules (Alfa Aesar, 99.9%) onto the graphene-covered Cu(111) substrate at room temperature by thermal evaporation. All STM and STS experiments were performed at a sample temperature of 1.2 K. Differential conductance was obtained by a lock-in technique with an ac modulation voltage of 50 meV (rms) at 727 kHz to the sample bias.

2.2 Calculation details

We used the Vienna *Ab initio* Simulation Package (VASP) to calculate the ground state of a many electrons system in the frame work of DFT.[10–13] The plane-wave basis set with an energy cut-off of 400 eV and the PBE-type gradient-corrected exchange–correlation potential were used.[14] The van der Waals interaction was implemented using the scheme of DFT-D2.[15] The ions were described by the projector augmented wave (PAW) potentials. To model the graphene/Cu template, we used a (4×4) supercell of graphene on the three layers of Cu(111). The stacked layers of C_{60}/graphene/Cu were separated from its replica along the perpendicular direction by more than 10 Å. In the self-consistent-field total energy calculations, the *k*-points were sampled over the uniform 3×3 grid in the Brillouin zone of the (4×4) two-dimensional graphene superlattice. All of the atomic positions were relaxed within residual forces smaller than 0.01 eV $Å^{-1}$. To simulate the STM images of the occupied and unoccupied states, we integrated the Kohn–Sham charge density in the energy window of 1.7 eV below or above the Fermi level, respectively.[16]

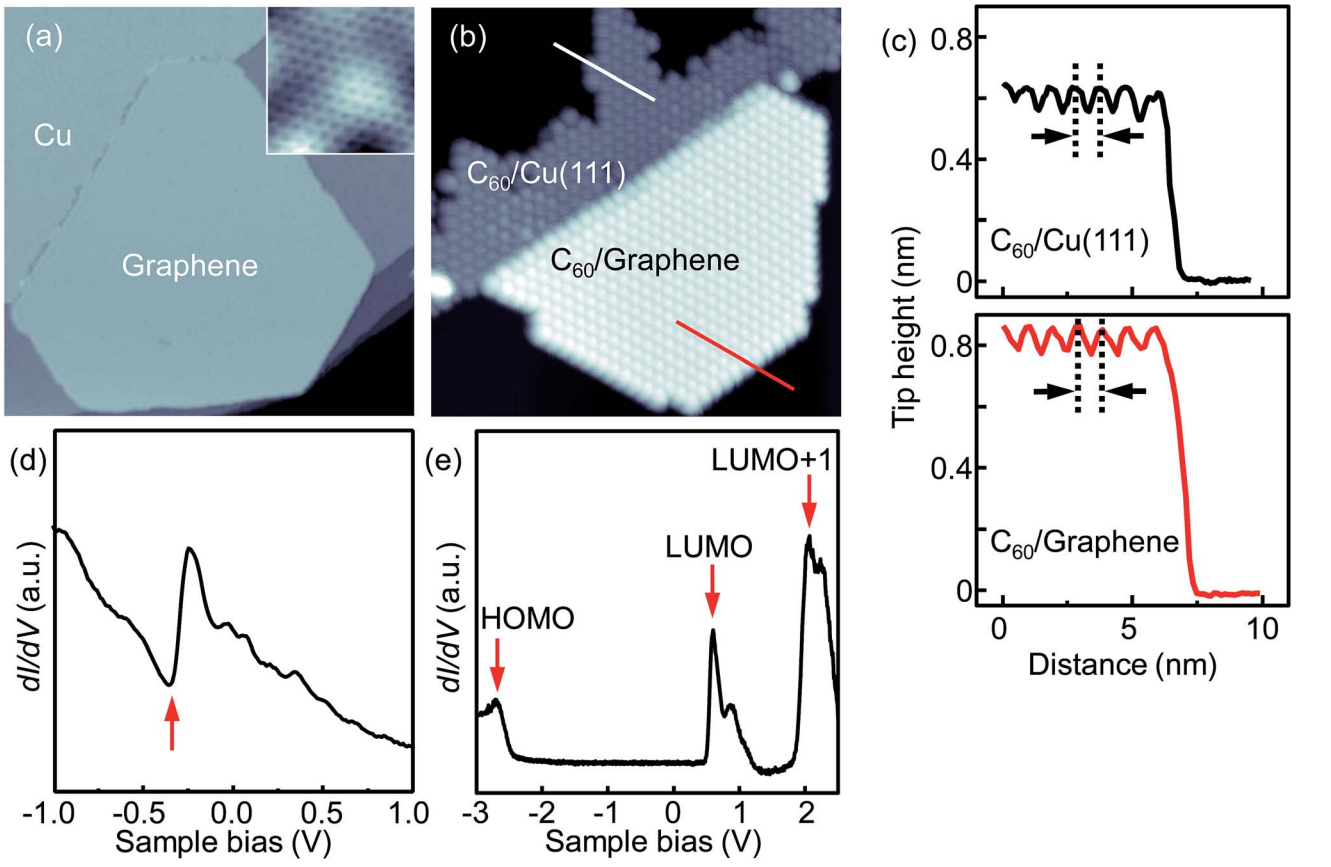

Fig. 1 Self-assembled fullerene molecules on graphene/Cu(111): STM images of (a) a single-layer graphene island on Cu(111) (100×100 nm^2, $V_{sample} = 0.1$ V, $I_t = 0.5$ nA) and (b) C_{60} molecules on Cu and graphene (100×100 nm^2, $V_{sample} = -0.2$ V, $I_t = 0.1$ nA). (c) Apparent height profiles of the C_{60} self-assembly on Cu(111) (upper) and on graphene (lower) taken along the white and red lines in (b). Differential conductance (d*I*/d*V*) measured from (d) graphene and (e) fullerene. The inset in (a) is a high-resolution STM image showing the honeycomb structure of graphene (2.4×2.4 nm^2, $V_{sample} = -0.01$ V, $I_t = 3.0$ nA). The arrow marked in (d) indicates the position of the Dirac point.

3. Results and discussion

Fig. 1a shows a STM topography image of a single-layer graphene island on a Cu(111) single crystal. We could routinely observe graphene islands, the sizes of which are smaller than ~100 nm. When we evaporated C_{60} molecules onto graphene/Cu(111) at room temperature, the fullerenes form an island of close-packed hexagonal structures both on graphene and on Cu surfaces (Fig. 1b). The apparent height of the C_{60} island on graphene is 8.5 ± 0.5 Å, higher than that on Cu(111) (6.3 ± 0.2 Å) in the STM images (Fig. 1c). The intermolecular distance between the fullerenes is 9.9 ± 0.2 Å on graphene and 10.3 ± 0.2 Å on Cu(111). In general, C_{60} molecules tend to form a hexagonal arrangement on the surface due to their lateral interaction. The different intermolecular distance originates from the different lattice constants of the underlying surfaces. The Cu–Cu bond length is 2.56 Å and the lattice constant of graphene is 2.46 Å. The van der Waals diameter of C_{60} is approximately 1.1 nm, which corresponds closely to nearly four unit cells of the underlying surfaces, *i.e.*, 10.2 Å for Cu(111) and 9.8 Å for graphene, indicating that the monolayer of C_{60} molecules on graphene and Cu(111) is arranged in a (4 × 4) superstructure.

The electronic structures of graphene and fullerene were measured by scanning tunnelling spectroscopy (STS). It should be noted that the Dirac point of graphene is located at −350 meV; that is, the Fermi level is shifted toward the unoccupied states (Fig. 1d). It is well known that the Dirac point shift of graphene is strongly influenced by the underlying substrate.[17–20] The charge transfer between graphene and the substrate results in the electron or hole doping of graphene. In our STS result, the Fermi level shift toward the unoccupied states indicates the n-type doping of graphene by the electron transfer from Cu to graphene. The STS of the fullerene on graphene shows well-defined peaks at −2.7, 0.7, and 2.1 V, which correspond to the highest occupied molecular orbital (HOMO), the lowest unoccupied molecular orbital (LUMO), and the LUMO+1 states of fullerene, respectively. Each peak position is related to the alignment of the molecular resonances of the C_{60} molecules. The measured HOMO–LUMO gap is ~3.4 eV, which is larger than that of fullerene on a metal surface.[21–23] Fullerene has a high electron affinity of 2.7 eV (ref. 24) and a bandgap energy of 4.9 eV.[25–27] When fullerenes form an island on a metal surface, the HOMO–LUMO gap is reduced compared to that of free C_{60} owing to the charge screening by neighbouring molecules and the metal surface.[22,28,29] On graphene, however, the electronic states of the C_{60} molecules are decoupled from the substrate. Therefore, the screening effect of the substrate is negligible on graphene. Recently, many researchers have studied C_{60} molecules on graphene synthesized on various surfaces.[30–35] A similar decoupling effect of graphene was reported by Cho *et al.*[31] On graphene/SiC(0001), C_{60} has a large HOMO–LUMO energy gap of 3.5 eV, which is slightly larger than our result. On the other hand, when adsorbed C_{60} molecules are commensurate with the graphene moiré structure on Ru(0001), the LUMO states of C_{60} shift toward a lower energy level due to the large amount of surface trapping energy.[33] In our result, however, we could not find any influence of moiré patterns of graphene/Cu(111) on the adsorbed C_{60} molecules. It means that self-assembled fullerene molecules on graphene exhibit different adsorption behaviours and electronic structures, depending on the support of the graphene layer.

To determine the exact adsorption site of fullerenes on graphene, we obtained a high-resolution STM image of graphene near the edge of a C_{60} island (Fig. 2a). Evidently, C_{60} molecules are arranged in a (4 × 4) superstructure, with the centre of each fullerene molecule located at the mid-point of a C–C bond of graphene. Interestingly, all of the C_{60} molecules have the same submolecular structure on graphene; the brightest region is off-centred from the adsorption site at a positive sample bias (Fig. 2b). At a negative sample bias, fullerenes are imaged as having a three-lobed shape (Fig. 2c). In our result, nearly every fullerene inside an island has the same submolecular structure regardless of the island size (Fig. S1†), which suggests that all of

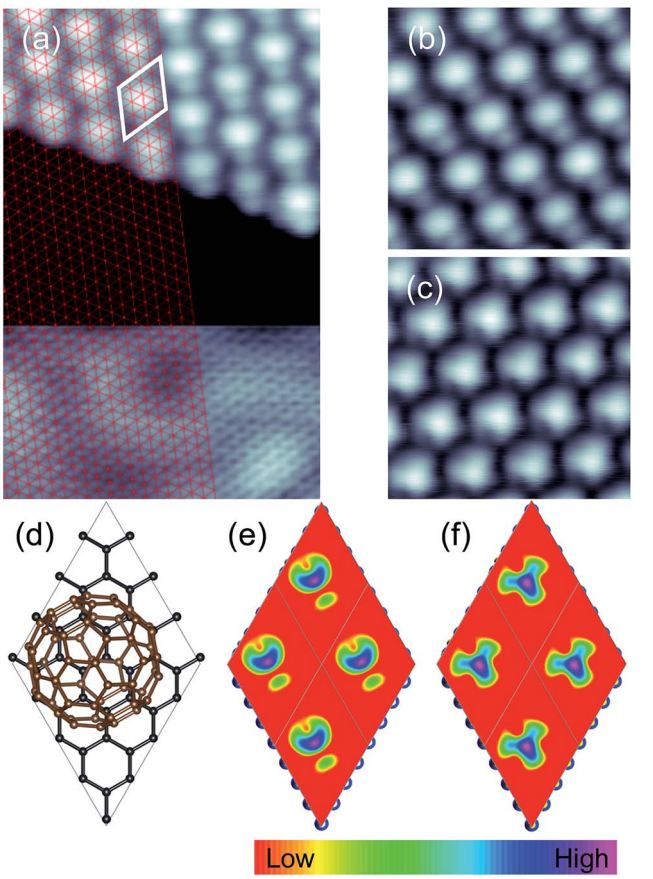

Fig. 2 Orientation of self-assembled C_{60} molecules on graphene: (a) STM image of C_{60} molecules on graphene (9.0 × 5.8 nm^2, top region: V_{sample} = 0.9 V and I_t = 100 pA, bottom region: V_{sample} = 3 mV and I_t = 2.0 nA). Bias dependence of STM images of C_{60} molecules acquired at I_t = 0.1 nA and V_{sample} = 0.9 V (b), and −2.7 V (c). (d) Optimized configuration of C_{60} on graphene/Cu as calculated by DFT calculations. The Cu layer underneath the graphene is not shown. The simulated STM images of four C_{60} molecules in a (4 × 4) superstructure for the unoccupied states (e) and for the occupied state (f). The red lines in (a) are drawn along the centre of carbon rings. The white rhombus in (a) indicates a (4 × 4) unit cell of graphene.

the fullerenes on graphene are equally oriented. During STM experiments, we always confirmed the cleanliness of the tip by measuring the STS on graphene or Cu(111) surfaces before acquiring the STM topographic images, since the molecular orbital of fullerenes could be imaged differently by the adsorption of C_{60} on the tip apex.[32] In the STM topography, the submolecular structure is shown to be related to the electronic structure of the fullerenes.[21,36] The 6:5 single bonds in fullerene, which have relatively low electron density, are shown to be brighter at a positive sample bias (the LUMO states), whereas the 6:6 double bonds are imaged as protrusions at a negative sample bias (the HOMO states). In order to confirm the precise configurations of fullerene, we performed the DFT calculations on our system. Considering the symmetry of C_{60}, there are five possible orientations with respect to the top of its cage: a carbon atom (CA), a hexagon (H), a pentagon (P), a 6:5 bond (H:P), and a 6:6 bond (H:H). Among these orientations, CA exhibits the best agreement with the experimental results. Fig. 2d shows the equilibrium configuration of C_{60}, where a carbon atom of fullerene is located at the mid-point of a C–C bond of graphene. For this orientation, the calculated HOMO and LUMO images are identical to the experimental results (Fig. 2e and f).

In previous STM studies of C_{60} molecules on surfaces, fullerenes in general showed H, H:P, H:H and P orientations in self-assembled islands.[31,32,37,38] We also observed that the orientation of C_{60} molecules on Cu(111), unlike those on graphene, was not uniform. Fig. 3a shows the calculated binding energy of C_{60} islands on graphene for the H:P, P and CA orientations. The CA orientation reveals the lowest energy of −1.787 eV, which means that the configuration of C_{60} molecules in our experimental result is the most stable in terms of energy. There are two major interactions that determine the equilibrium superstructures of self-assembled molecular adsorbates: (1) the interaction between the molecules and the substrate and (2) the interaction among the molecules. We calculated the binding energy of C_{60} aggregates without a support to examine the effect of the substrate. In this case, the CA orientation showed the lowest binding energy as well, while the H:P orientation showed a lower binding energy than the P orientation. The energy difference between Fig. 3a and b represents the adsorption energy of C_{60} on graphene/Cu(111). The adsorption energies of C_{60} in the CA, P and H:P orientations are −0.991, −1.047, and −0.977 eV, respectively. This signifies that the C_{60}–graphene interaction is the strongest for the P orientation.

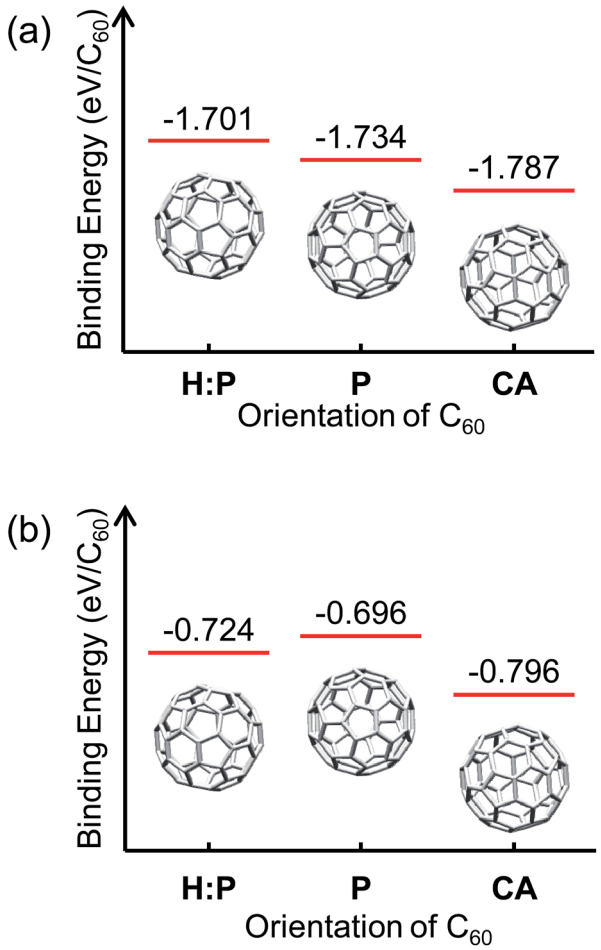

Fig. 3 Binding energy per C_{60} for various orientations, *i.e.*, H:P, P, and CA: (a) C_{60} molecules in a (4 × 4) superstructure on graphene/Cu(111) and (b) C_{60} molecules without a substrate.

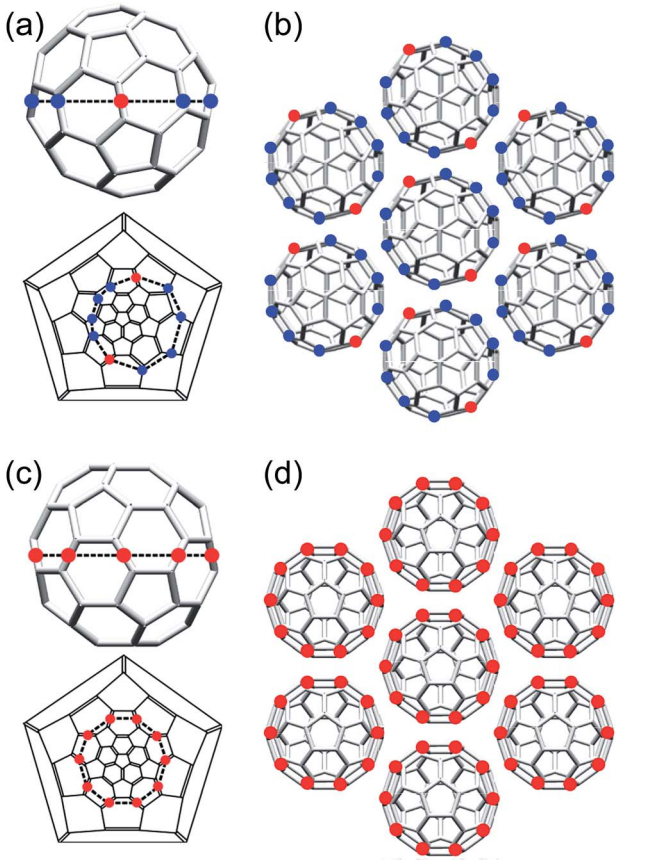

Fig. 4 Intermolecular interaction among self-assembled C_{60} molecules on graphene/Cu(111): side view and Schlegel diagram of C_{60} in the CA orientation (a), and in the P orientation (c). Distribution of e-poor and e-rich C–C bonds in the circumference of self-assembled C_{60} molecules in the CA orientation (b), and in the P orientation (d). Blue and red dots indicate the e-poor and e-rich C–C bonds, respectively.

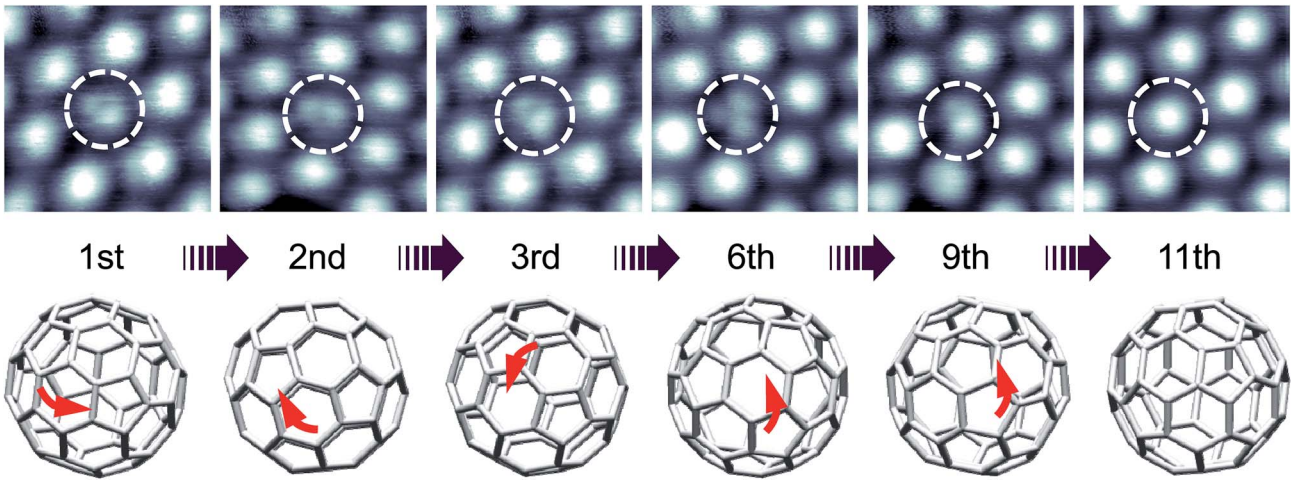

Fig. 5 Reorientation of a disordered C_{60} during successive scans: Upper: a series of STM images (3×3 nm^2, $V_{sample} = 1.5$ V, and $I_t = 50$ pA). The disordered fullerenes are marked by the dotted circles. Lower: the orientation of fullerenes as marked in the upper images.

As noted above, a pentagon ring of C_{60} is an electron-poor region, and the graphene on Cu(111) is doped by electrons due to the charge transfer. Hence, the electrostatic interaction between C_{60} and graphene/Cu(111) is the strongest for the configuration with a pentagon ring of fullerene facing a graphene surface.

Our experimental and computational results reveal that the C_{60}–C_{60} intermolecular interaction plays a more important role in determining the equilibrium orientation of each molecule than the C_{60}–graphene interaction. Why does the CA orientation have strong intermolecular interactions? Fig. 4a shows a side view and a Schlegel diagram of fullerene in the CA orientation, which illustrates the distribution of C–C bonds in the circumference of a fullerene. There are two electron-rich (e-rich) double bonds and eight electron-poor (e-poor) single bonds. The strong attractive Coulomb interaction may favour the alignment of e-rich and e-poor bonds. In addition, the repulsive force between e-poor bonds also affects the azimuthal orientations of fullerenes. Considering the symmetry of the molecules, we can confirm that the Coulomb interaction among molecules becomes stronger when the fullerenes are arranged in the same way as our experimental result (Fig. 4b). On the other hand, all of the C–C bonds in the circumference are e-rich double bonds in the P orientation (Fig. 4c and d), which induces only repulsive force among the molecules regardless of the azimuthal orientation. We expect that the isolated C_{60} molecules may have lower energy for the P orientation upon adsorption. When they are assembled into an island to form a (4×4) structure, a 20.3° tilt of C_{60} molecules from the P orientation to the CA orientation can minimize the intermolecular Coulomb energy.

Although most C_{60} molecules in islands have the same orientation, we could, by chance, find a disordered fullerene in a C_{60} island (Fig. 5). Interestingly, it changes its orientation during successive scanning processes, which means that the rotation of this unstable fullerene is induced by the STM tip. Finally, it finds a stable orientation of CA after the 11th scan, at which point it no longer changes its orientation. It is difficult to estimate the energy barrier associated with the rotation of the fullerene inside islands, but it appears that the strong electric field in the gap below the tip or tunnelling electrons from the tip would be sufficient to overcome the rotational energy barrier. We recognize from this result that the CA orientation is the most stable orientation and that a strong intermolecular interaction is the main origin that determines the individual orientations of fullerenes on graphene/Cu(111).

4. Conclusion

In summary, we have successfully resolved the stable configuration of self-assembled fullerene molecules on graphene/Cu(111) using STM and DFT calculations. Fullerene molecules absorb at the mid-point of C–C bonds of graphene, forming (4×4) superstructures. Furthermore, we observed the homogeneous alignment of C_{60} molecules inside islands on graphene. The n-doped graphene on Cu(111) prefers the P orientation of a fullerene energetically; however, the Coulomb interaction among neighbouring fullerenes is strong enough to align the C_{60} molecules in the final orientation of CA. We believe that our findings have demonstrated the importance of intermolecular and molecule–substrate interactions in determining equilibrium configurations for weakly adsorbed molecular systems, thus also providing a useful basis for developing carbon-based electronic devices in the future.

Acknowledgements

This research was supported by the Basic Science Research Program through the National Research Foundation of Korea (NRF) funded by the Ministry of Science, ICT & Future Planning (Grant no. 2011-0014807), by the year of 2011 Research Fund of UNIST (Grant no. 1.110009.01), by a UNIST Future Challenge Project (Grant no. 1.140026.01), and by the KIST-UNIST Ulsan

Center (KUUC) for Convergent Materials. This work has benefited from the use of the facilities at UNIST Central Research Facilities.

References

1 A. Geim and K. Novoselov, *Nat. Mater.*, 2007, **6**, 183–191.
2 A. H. Castro Neto, F. Guinea, N. M. R. Peres, K. S. Novoselov and A. K. Geim, *Rev. Mod. Phys.*, 2009, **81**, 109–162.
3 M. J. Allen, V. C. Tung and R. B. Kaner, *Chem. Rev.*, 2010, **110**, 132–145.
4 M. Batzill, *Surf. Sci. Rep.*, 2012, **67**, 83–115.
5 M. Funahashi, F. P. Zhang and N. Tamaoki, *Adv. Mater.*, 2007, **19**, 353–358.
6 N. Matín, L. Sánchez, M. Á. Herranz, B. Illescas and D. M. Guldi, *Acc. Chem. Res.*, 2007, **40**, 1015–1024.
7 K. Hutchison, J. Gao, G. Schick, Y. Rubin and F. Wudl, *J. Am. Chem. Soc.*, 1999, **121**, 5611–5612.
8 X. Li, W. Cai, J. An, S. Kim, J. Nah, D. Yang, R. Piner, A. Velamakanni, I. Jung, E. Tutuc, S. K. Banerjee, L. Colombo and R. S. Ruoff, *Science*, 2009, **324**, 1312–1314.
9 Z. R. Robinson, P. Tyagi, T. R. Mowll, C. A. Ventrice, Jr and J. B. Hannon, *Phys. Rev. B: Condens. Matter Mater. Phys.*, 2012, **86**, 235413.
10 P. Hohenberg and W. Kohn, *Phys. Rev. B: Condens. Matter Mater. Phys.*, 1964, **136**, B864–B871.
11 W. Kohn and L. J. Sham, *Phys. Rev.*, 1965, **140**, A1133–A1138.
12 G. Kresse and J. Furthmüller, *Phys. Rev. B: Condens. Matter Mater. Phys.*, 1996, **54**, 11169–11186.
13 G. Kresse and J. Furthmüller, *Comput. Mater. Sci.*, 1996, **6**, 15–50.
14 J. P. Perdew, K. Burke and M. Ernzerhof, *Phys. Rev. Lett.*, 1996, **77**, 3865–3868.
15 S. Grimme, *J. Comput. Chem.*, 2006, **27**, 1787–1799.
16 J. Tersoff and D. R. Hamann, *Phys. Rev. B: Condens. Matter Mater. Phys.*, 1985, **31**, 805–813.
17 G. Giovannetti, P. A. Khomyakov, G. Brocks, V. M. Karpan, J. van den Brink and P. J. Kelly, *Phys. Rev. Lett.*, 2008, **101**, 026803.
18 P. A. Khomyakov, G. Giovannetti, P. C. Rusu, G. Brocks, J. van den Brink and P. J. Kelly, *Phys. Rev. B: Condens. Matter Mater. Phys.*, 2009, **79**, 195425.
19 L. Gao, J. R. Guest and N. P. Guisinger, *Nano Lett.*, 2010, **10**, 3512–3516.
20 A. L. Vázquez de Parga, F. Calleja, B. Borca, M. C. G. Passeggi, Jr, J. J. Hinarejos, F. Guinea and R. Miranda, *Phys. Rev. Lett.*, 2008, **100**, 056807.
21 M. Grobis, X. Lu and M. F. Crommie, *Phys. Rev. B: Condens. Matter Mater. Phys.*, 2002, **66**, 161408.
22 X. Lu, M. Grobis, K. H. Khoo, S. G. Louie and M. F. Crommie, *Phys. Rev. B: Condens. Matter Mater. Phys.*, 2004, **70**, 115418.
23 G. Schull, N. Néel, M. Becker, J. Kröger and R. Berndt, *New J. Phys.*, 2008, **10**, 065012.
24 H. W. Kroto, J. R. Heath, S. C. O'Brien, R. F. Curl and R. E. Smalley, *Nature*, 1985, **318**, 162–163.
25 T. R. Ohno, Y. Chen, S. E. Harvey, G. H. Kroll, J. H. Weaver, R. E. Haufler and R. E. Smalley, *Phys. Rev. B: Condens. Matter Mater. Phys.*, 1991, **44**, 13747–13755.
26 S. H. Yang, C. L. Pettiette, J. Conceicao, O. Cheshnovsky and R. E. Smalley, *Chem. Phys. Lett.*, 1987, **139**, 233–238.
27 I. V. Hertel, H. Steger, J. de Vries, B. Weisser, C. Menzel, B. Kamke and W. Kamkw, *Phys. Rev. Lett.*, 1992, **68**, 784–787.
28 I. F. Torrente, K. J. Franke and J. I. Pascual, *J. Phys.: Condens. Matter*, 2008, **20**, 184001.
29 C. Silien, N. A. Pradhan, W. Ho and P. A. Thiry, *Phys. Rev. B: Condens. Matter Mater. Phys.*, 2004, **69**, 115434.
30 H. T. Zhou, J. H. Mao, G. Li, Y. L. Wang, X. L. Feng, S. X. Du, K. Müllen and H.-J. Gao, *Appl. Phys. Lett.*, 2011, **99**, 153101.
31 J. Cho, J. Smerdon, L. Gao, O. Süzer, J. Guest and N. Guisinger, *Nano Lett.*, 2012, **12**, 3018–3024.
32 M. Švec, P. Merino, Y. J. Dappe, C. González, E. Abad, P. Jelínek and J. A. Martín-Gago, *Phys. Rev. B: Condens. Matter Mater. Phys.*, 2012, **86**, 121407.
33 J. Lu, P. S. E. Yeo, Y. Zheng, Z. Yang, Q. Bao, C. K. Gan and K. P. Loh, *ACS Nano*, 2012, **6**, 944–950.
34 G. Li, H. T. Zhou, L. D. Pan, Y. Zhang, J. H. Mao, Q. Zou, H. M. Guo, Y. L. Wang, S. X. Du and H.-J. Gao, *Appl. Phys. Lett.*, 2012, **100**, 013304.
35 M. Chen, H. Zhou, F. Yu, H. Yang, G. Wang, J. He and L. Sun, *Nanoscale*, 2013, **5**, 8359–8362.
36 X. Lu, M. Grobis, K. H. Khoo, S. G. Louie and M. F. Crommie, *Phys. Rev. Lett.*, 2003, **90**, 096802.
37 J. A. Larsson, S. D. Elliott, J. C. Greer, J. Repp, G. Meyer and R. Allenspach, *Phys. Rev. B: Condens. Matter Mater. Phys.*, 2008, **77**, 115434.
38 D. R. Daughton and J. A. Gupta, *Appl. Phys. Lett.*, 2011, **98**, 133303.